# Heavy Quark Production and Spectroscopy at HERA

Uri Karshon [1]

*Weizmann Institute of Science, Israel*

**Abstract.** Production of final states containing open charm ($c$) and beauty ($b$) quarks at HERA is reviewed. Photoproduction (PHP) of the charm meson resonances $D^*$, $D^0$ and $D_s$, as well as $D^*$ production in the deep inelastic scattering (DIS) regime, are measured and compared to QCD predictions. The excited charm mesons $D_1^0(2420)$, $D_2^{*0}(2460)$ and $D_{s1}^{\pm}(2536)$ have been observed and the rates of charm quarks hadronising to these mesons were extracted. A search for radially excited charm mesons has been performed. PHP and DIS beauty cross sections are higher than expected in next-to-leading order (NLO) QCD.

## INTRODUCTION

The HERA e-p collider accelerates electrons (or positrons) and protons to energies of $E_e = 27.5\,\text{GeV}$ and $E_p = 920\,\text{GeV}$ ($820\,\text{GeV}$ until 1997), respectively. The H1 and ZEUS experiments are located at two collision points along the circulating beams. The incoming $e^{\pm}$ interacts with the proton by first radiating a virtual photon. The photon is either quasi-real with $Q^2 < 1\,\text{GeV}^2$ and $Q^2_{median} \approx 3 \cdot 10^{-4}\,\text{GeV}^2$ (PHP regime) or highly virtual ($Q^2 > 1\,\text{GeV}^2$ - DIS regime).

The large masses of the heavy quarks (HQ) $c$ and $b$ provide a "hard" scale needed for the comparison of data to QCD predictions. In leading-order (LO) QCD, two types of processes are responsible for the PHP of HQ's: Direct photon processes, where the photon interacts as a point-like particle with a parton from the incoming proton, and resolved photon processes, where a parton from the photon partonic structure scatters off a parton from the proton. Heavy quarks ($Q$) present in the parton distributions of the photon lead to LO resolved processes, such as $Qg \to Qg$ (where g is a gluon), which are called heavy flavour excitation. In NLO calculations, only the sum of direct and resolved processes is unambiguously defined.

Two different NLO calculations are available for comparison with measurements of HQ PHP at HERA: 1) a fixed-order ("massive") approach [1, 2], where HQ's are produced only dynamically in the hard subprocess. This calculation is expected to become less accurate when $p_\perp^2 >> m_Q^2$, where $p_\perp$ and $m_Q$ are the transverse momentum and mass of the HQ; 2) a resummed ("massless") approach [3, 4], where the massless HQ's from the photon and proton parton distributions are used explicitly. This calculation is expected to yield better results as $p_\perp^2 >> m_Q^2$.

[1] On behalf of the H1 and ZEUS Collaborations

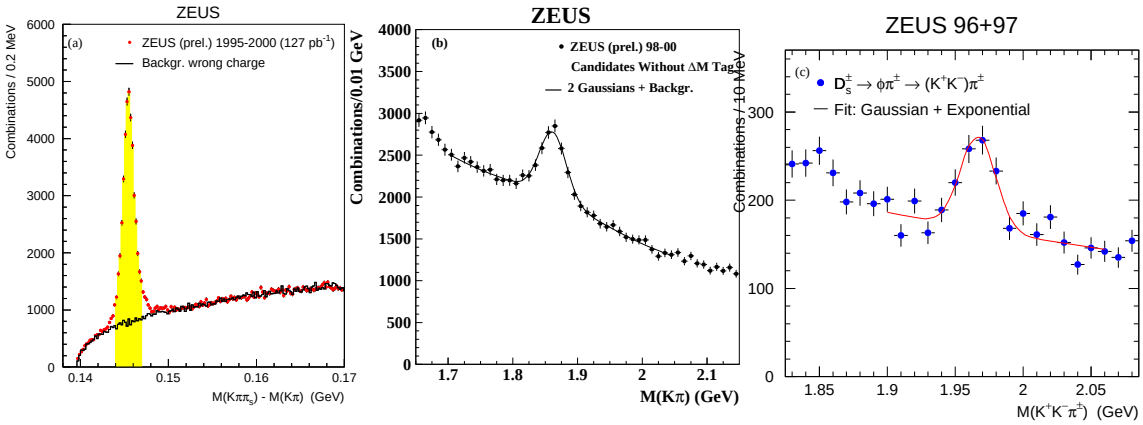


**FIGURE 1.** (a) $M(K\pi\pi_S) - M(K\pi)$ distribution in the $D^0$ mass region (full dots). The histogram is the distribution for wrong charge combinations. (b) $M(K^\pm\pi^\mp)$ distribution for events excluding the $D^{*\pm}$ region. The solid curve is a fit to two Gaussian shapes for the right and wrong $K$ mass assignments plus a sum of exponential and linear backgrounds. (c) $M(K^+K^-\pi^\pm)$ distribution for events inside the $\phi$ mass range ($1.0115 < M(K^+K^-) < 1.0275\,\text{GeV}$). The solid curve is a fit to a Gaussian resonance plus an exponential background.

## PRODUCTION OF $D^{*\pm}$, $D^0$ AND $D_S$ MESONS

The charmed meson $D^{*\pm}$ has been reconstructed via its decay chain $D^{*+} \to D^0\pi_S^+ \to (K^-\pi^+)\pi_S^+$ (+ c.c.). Fig. 1(a) shows the mass difference distribution, $\Delta M = M(K\pi\pi_S) - M(K\pi)$, in the $D^0$ mass region $1.83 < M(K\pi) < 1.90\,\text{GeV}$ in the kinematic range $p_\perp^{D^*} > 2\,\text{GeV}$ and $|\eta^{D^*}| < 1.5$, where $p_\perp$ is the transverse momentum and $\eta = -\ln\tan(\theta/2)$ is the pseudorapidity. The polar angle, $\theta$, is defined with respect to the proton beam direction. The plot includes PHP and DIS ZEUS data collected during 1995-2000 [5]. A clear $D^{*\pm}$ signal is seen (dots) on top of a small combinatorial background, estimated by wrong charge combinations (histogram), where both $D^0$ tracks have the same charge and $\pi_S$ has the opposite charge. Defining $D^{*\pm}$ candidates as events with $0.144 < \Delta M < 0.147\,\text{GeV}$, a signal of $31350 \pm 240$ $D^{*\pm}$ mesons was found after background subtraction.

Inclusive production of charm hadrons other than the $D^{*\pm}$ have also been observed. The $M(K^\pm\pi^\mp)$ distribution for PHP events excluding the $D^{*\pm}$ region ($0.143 < \Delta M < 0.148\,\text{GeV}$) is shown in Fig. 1(b) for a restricted kinematic region, using a ZEUS event sample with integrated luminosity $\mathcal{L} = 66\,\text{pb}^{-1}$ [6]. A clear $D^0$ signal is seen. The production ratio, $P_v$, of vector to pseudoscalar+vector ground state (orbital angular momentum $L = 0$ of the $c\bar{q}$ system) charm mesons can be approximated by $P_v = (\sigma(D^0)/\sigma(D^{*+}) - B_{D^{*+}\to D^0\pi})^{-1}$, where $\sigma(D^0)$ and $\sigma(D^{*+})$ are, respectively, the inclusive $D^0$ and $D^{*\pm}$ cross sections and $B_{D^{*+}\to D^0\pi}$ is the $D^{*+}$ branching ratio to $D^0\pi^+$. Using also the $D^0$ signal from events in the $D^*$ region with the same cuts yields the preliminary result $P_v = 0.546 \pm 0.045(\text{stat.}) \pm 0.028(\text{syst.})$. This measurement is in good agreement with the $e^+e^-$ annihilation results, $0.57 \pm 0.05$ and $0.595 \pm 0.045$ [7], supporting the universality of charm fragmentation.

Using a ZEUS PHP sample with $38\,\text{pb}^{-1}$ in a restricted kinematic region, a $D_s$

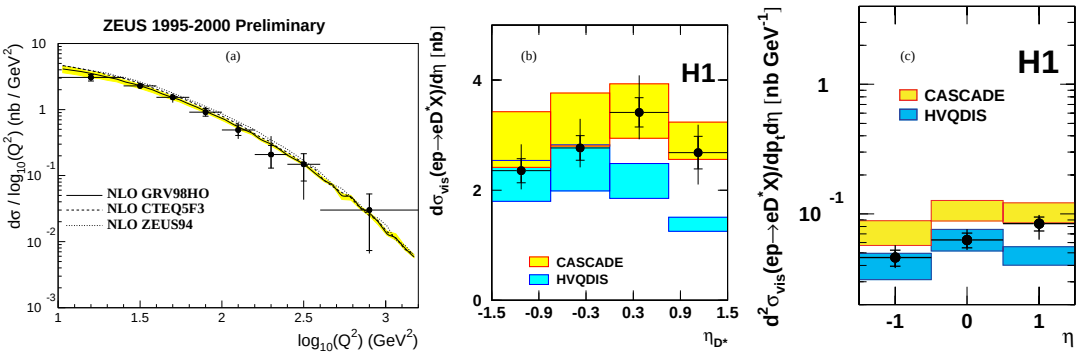


**FIGURE 2.** (a) Differential $D^*$ cross section in $\log_{10}(Q^2)$ compared to the NLO HVQDIS calculations with different structure function parametrisations. (b) Differential $D^*$ DIS ($1 < Q^2 < 100\,\text{GeV}^2$) cross section in $\eta^{D^*}$ compared with HVQDIS (lower shaded band) and CASCADE (upper shaded band) predictions. (c) Same as b) for $4 < p_\perp^{D^*} < 10\,\text{GeV}$.

signal is seen (Fig. 1(c)) in the $K^+K^-\pi^\pm$ mass distribution for events where $M(K^+K^-)$ is in the $\phi$ mass range [8]. The ratio of the $D_s$ to $D^*$ cross sections in identical kinematic regions was measured to be $\sigma_{ep\to D_sX}/\sigma_{ep\to D^*X} = 0.41 \pm 0.07\,(\text{stat.})^{+0.03}_{-0.05}\,(\text{syst.}) \pm 0.10\,(\text{br.})$, where the last error is due to the uncertainty in the $D_s \to \phi\pi$ branching ratio. This result is in good agreement with the ratio $f(c \to D_s^+) \,/\, f(c \to D^{*+}) = 0.43 \pm 0.04 \pm 0.11\,(\text{br.})$ obtained [8, 9] from $e^+e^-$ experiments, again confirming the universality of charm fragmentation.

## $D^{*\pm}$ Production in DIS

Open charm production in the DIS regime is dominated by boson-gluon fusion (BGF) processes, where the boson (gluon) is emitted from the incoming electron (proton). Fixed-order NLO perturbative QCD (pQCD) calculations are available in the form of a Monte Carlo (MC) integrator (HVQDIS) [10]. The ZEUS preliminary $D^*$ differential cross section in $Q^2$, using a sample of $\mathcal{L} = 82.6\,\text{pb}^{-1}$, is shown in Fig. 2(a) for the kinematic region $Q^2 > 10\,\text{GeV}^2$, $p_\perp^{D^*} > 1.5\,\text{GeV}$ and $|\eta^{D^*}| < 1.5$ [11]. The distribution compares well with the HVQDIS calculations, using 3 different parton distribution functions in the proton and a charm quark mass range $1.3 < m_c < 1.6\,\text{GeV}$. For $Q^2 >> m_c^2$, resummed NLO calculations should be superior. However, up to $Q^2 \approx 1000\,\text{GeV}^2$, the data is nicely described by the fixed-order scheme. The $D^{*\pm}$ cross sections were also measured separately for $e^+$ and $e^-$ beams [12]. Integrated over $Q^2 > 20\,\text{GeV}^2$, the $e^-p$ cross section is higher than that for $e^+p$ by $\approx 3$ standard deviations. Both results are compatible with the predictions within the theoretical uncertainties.

The H1 Collaboration has measured $D^{*\pm}$ production in DIS, using $\mathcal{L} = 18.6\,\text{pb}^{-1}$, in a kinematic region $1 < Q^2 < 100\,\text{GeV}^2$, $p_\perp^{D^*} > 1.5\,\text{GeV}$ and $|\eta^{D^*}| < 1.5$ [13]. The differential cross section in $\eta^{D^*}$ is compared in Figs. 2(b-c) to HVQDIS [10] and to CASCADE [14] calculations, which implement a version of the CCFM evolution scheme [15]. The shaded bands reflect the uncertainties in the predictions due to $m_c$ ($1.3 - 1.5\,\text{GeV}$) and the allowed fragmentation parameters. CASCADE shows better agreement with the overall $\eta^{D^*}$ distribution (Fig. 2(b)), while the HVQDIS prediction is

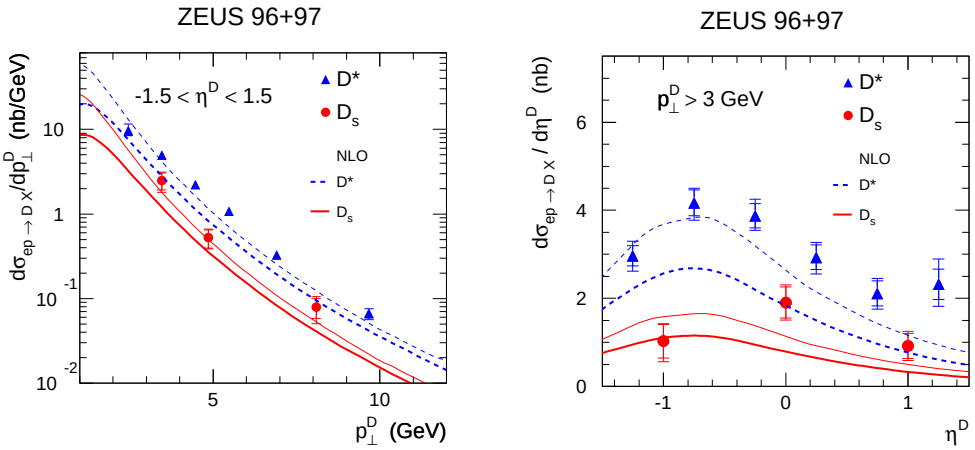


**FIGURE 3.** Differential cross sections in $p_\perp^D$ and $\eta^D$, where $D$ stands for $D^*$ or $D_s$. The $D_s$ (dots) and $D^*$ (triangles) data are compared with NLO predictions for $D_s$ (full curves) and $D^*$ (dashed curves) with two parameter settings: $m_c = 1.5\,\text{GeV}$, $\mu_R = m_\perp$ (thick curves) and $m_c = 1.2\,\text{GeV}$, $\mu_R = 0.5 m_\perp$ (thin curves). Here $\mu_R$ is the renormalisation scale and $m_\perp = \sqrt{m_c^2 + p_\perp^2}$.

too low for the forward region. CASCADE agrees poorly with the data at the low-$\eta^{D^*}$ high-$p_\perp^{D^*}$ region (Fig. 2(c)).

## Photoproduction of charm mesons

Differential $D_s^\pm$ cross sections in $p_\perp$ and $\eta$ [8] were compared to those for $D^{*\pm}$ [16] in the same kinematic region $Q^2 < 1\,\text{GeV}^2$, $130 < W < 280\,\text{GeV}$, $p_\perp^D > 3\,\text{GeV}$ and $|\eta^D| < 1.5$ , where $W$ is the $\gamma p$ centre-of-mass energy, and with fixed-order NLO calculations [17] (Fig. 3). The cross sections for both cases are above the predictions, in particular for $\eta$ in the forward (proton) direction. NLO resummed predictions [3] are closer to the $D^*$ data [16], but still too low for high $\eta$. Using different photon parton density functions shows some sensitivity to the parton density parametrisation of the photon. A tree-level pQCD calculation [18], where the $c\bar{q}$ state is hadronised rather than the $c$ quark, gives a better agreement with the data compared to the NLO calculations.

## $D^{*\pm}$ and Associated Dijets

Events with a reconstructed $D^{*\pm}$ and at least 2 hadron jets ("dijet event") enable one to study the photon structure, in particular its charm content. $D^{*\pm}$ candidates with $p_\perp^{D^*} > 3\,\text{GeV}$ and $|\eta^{D^*}| < 1.5$ have been selected. The two jets with the highest transverse energy, $E_T$, in the pseudorapidity range $|\eta^{jet}| < 2.4$ are required to have $E_T^{jet1}$ and $E_T^{jet2}$ above certain values. The fraction of the photon momentum participating in the dijet production, $x_\gamma^{\text{OBS}}$ , is defined as $x_\gamma^{\text{OBS}} = \frac{\Sigma_{\text{jets}} E_T e^{-\eta}}{2yE_e}$, where $y$ is approximately the fraction of incoming electron energy carried by the photon. In LO QCD, direct processes have $x_\gamma^{\text{OBS}} = 1$ while resolved processes have $x_\gamma^{\text{OBS}} < 1$. Samples enriched with direct (resolved) events are separated by a cut $x_\gamma^{\text{OBS}} > 0.75 (< 0.75)$.

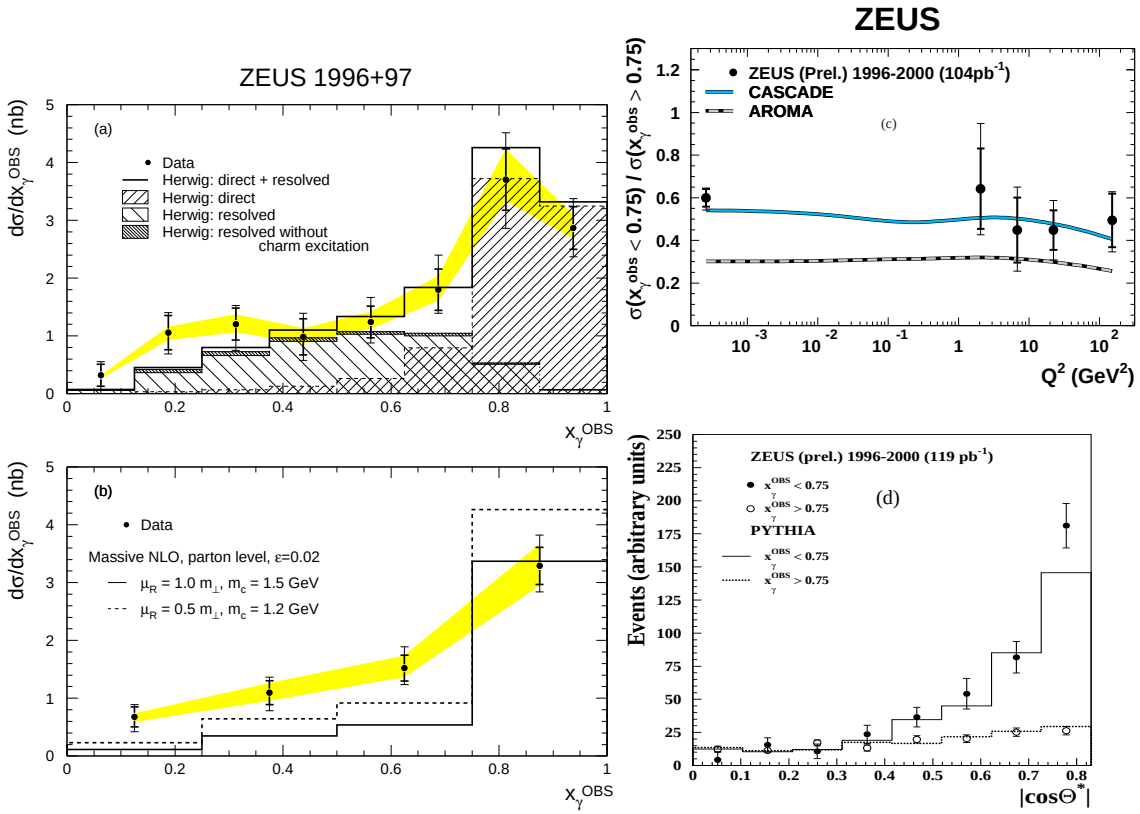


**FIGURE 4.** (a-b) Differential cross sections $d\sigma/dx_\gamma^{\rm OBS}$ for dijets with an associated $D^*$ in the PHP range with $E_T^{jet1} > 7\,$GeV and $E_T^{jet2} > 6\,$GeV. In (a), the experimental data (dots) are compared to the expectations of the HERWIG MC simulation, normalised to the data, for LO-direct (right hatched), LO-resolved (left hatched), LO-resolved without charm excitation (dense hatched) and the sum of LO-direct and LO-resolved photon contributions (full histogram). In (b), the data are compared with a parton level NLO fixed-order calculation. (c) Ratio of low to high $x_\gamma^{\rm OBS}$ for $D^*$ dijet events with $E_T^{jet1,2} > 7.5,\ 6.5\,$GeV vs. $Q^2$ compared to the AROMA and CASCADE MC's. The left-hand point is due to PHP events. (d) Differential distributions in $|\cos\theta^*|$ for $D^*$ dijet events with $E_T^{jet1,2} > 5\,$GeV. Data (dots) and PYTHIA MC (lines) are shown separately for direct- (open dots/dashed lines) and resolved- (black dots/full lines) photon events. All distributions are normalised to the resolved data in the lowest 4 bins.

Differential cross sections in $x_\gamma^{\rm OBS}$ for ZEUS measurements with $\mathcal{L} = 37\,{\rm pb}^{-1}$ are shown in Fig. 4(a-b) [16] and compared with LO MC simulation and NLO fixed-order calculation. The peak at high $x_\gamma^{\rm OBS}$ is due to the LO-direct BGF process. The low $x_\gamma^{\rm OBS}$ tail comes from LO-resolved processes, dominated by photon charm excitation. The shape of the $x_\gamma^{\rm OBS}$ distribution is in good agreement with the MC simulation with $\approx 40\%$ resolved contribution (Fig. 4(a)). The fixed-order NLO calculation lies below the data at low $x_\gamma^{\rm OBS}$ values (Fig. 4(b)). This could be due to the fact that no explicit charm excitation component exists in this calculation.

The dependence of the virtual-photon structure on its virtuality, $Q^2$, has been studied with ZEUS dijet events containing a $D^*$ [19]. The cross section ratio $R = \sigma(x_\gamma^{\rm OBS} < 0.75)/\sigma(x_\gamma^{\rm OBS} > 0.75)$ as a function of $Q^2$ is shown in Fig. 4(c) to be approximately

constant up to $Q^2 \approx 200\,\mathrm{GeV}^2$, contrary to the no-charm-tag case, where $R$ falls with increasing $Q^2$. The data are compared to two MC models which implement no specific partonic structure for the photon, generating all low $x_\gamma^{\mathrm{OBS}}$ events from parton showers in two different schemes. The AROMA [20] model, which implements the DGLAP evolution scheme [21], lies below the data. The CASCADE results [14] are much closer to the data.

The angular distributions, $dN/d|\cos\theta^*|$, of dijet events containing a $D^*$ in the PHP regime have been measured by ZEUS [22]. Here $\theta^*$ is the angle between the jet-jet axis and the beam direction in the dijet rest frame. The results are shown in Fig. 4(d) separately for direct and resolved photon events. The resolved processes peak at high $|\cos\theta^*|$, in agreement with LO MC predictions, as expected for dominant gluon exchange. The direct processes are much flatter in $|\cos\theta^*|$, consistent with quark exchange. The steep rise towards high $|\cos\theta^*|$ of the resolved charm events provides evidence that the bulk of the resolved contribution is due to charm excitation in the photon.

## EXCITED CHARM MESONS

P-wave charm mesons (L=1 of the $c\bar{q}$ system) can decay into L=0 states plus a $\pi$ or a $K$ [23]. They are predicted [24] to appear in two doublets with total angular momentum j=3/2 (narrow states) or j=1/2 (broad states). Narrow states, $D_1(2420)$ and $D_2^*(2460)$, were observed in the $D^*\pi$ decay mode and identified as members of the j=3/2 doublet with spin-parity $J^P = 1^+$ and $2^+$, respectively [23]. A charm-strange excited meson, $D_{s1}^{\pm}(2536)$, was found in the $D^{*\pm}K_S^0$ final state [23].

### $D_1^0(2420)$ and $D_2^{*0}(2460)$ production

$D_1^0$ and $D_2^{*0}$ mesons were reconstructed by ZEUS [25] via their decays to $D^{*\pm}\pi_4^{\mp}$, followed by the $D^{*\pm}$ decays, $D^{*+} \to D^0\pi_S^+ \to (K^-\pi^+)\pi_S^+ (+c.c.)$. Fig. 5(a) shows the "extended" mass difference distribution, $M(K\pi\pi_S\pi_4) - M(K\pi\pi_S) + M(D^*)$, where $M(D^*)$ is the nominal $D^{*\pm}$ mass [23] (full dots). A clear excess is seen around the mass region of the $D_1^0(2420)$ and $D_2^{*0}(2460)$ mesons. No enhancement is seen for wrong charge combinations (dashed histogram), where $D^*$ and $\pi_4$ have the same charges. The solid curves in Figs. 5(a-b) are an unbinned likelihood fit to two Breit-Wigner shapes with masses and widths fixed to the nominal $D_1^0$ and $D_2^{*0}$ values [23], convoluted with a Gaussian function and multiplied by helicity spectrum functions for $J^P = 1^+$ and $2^+$ states, respectively. The background shape was parametrised by the form $x^\alpha \cdot exp(-\beta \cdot x + \gamma \cdot x^2)$, where $x = M(K\pi\pi_S\pi_4) - M(K\pi\pi_S) - M(\pi)$. The fitted curves describe the distribution reasonably well, except for a narrow enhancement near $2.4\,\mathrm{GeV}$ (Fig. 5(b)). In Fig. 5(c), a similar fit is shown with an additional Gaussian-shaped resonance with free mass and width. The fit yielded $211 \pm 49$ entries for the narrow enhancement with mass value $2398.1 \pm 2.1\,(\mathrm{stat.})^{+1.6}_{-0.8}\,(\mathrm{syst.})$ MeV. The width was consistent with the resolution expected from the tracking detector. The enhancement may indicate a new excited charm meson, a result of an interference effect or a statistical fluctuation. The number of reconstructed $D_1^0$ and $D_2^{*0}$ mesons in the 3-resonance fit are $526 \pm 65$ and

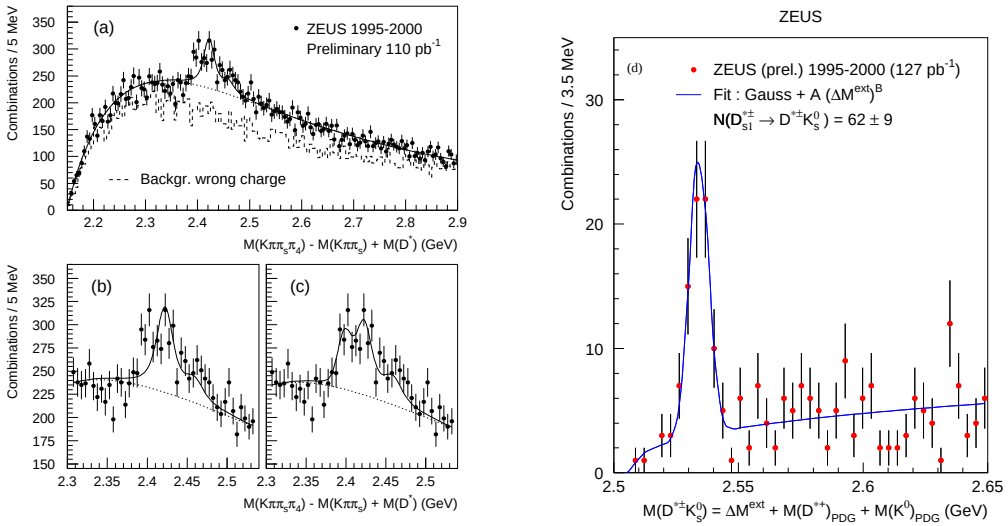


**FIGURE 5.** (a-c) Extended mass difference distribution for $D^{*\pm}$ candidates (full dots). The dashed histogram is for wrong charge cominations. The curves are the results of unbinned likelihood fits. In (a) and (b) the solid curves are a fit to background parametrisation and two Breit-Wigner distributions convoluted with a Gaussian function. In (c) an additional Gaussian-shaped resonance near $2.4\,\text{GeV}$ is assumed in the fit. The dotted curves are fitted shapes of the combinatorial background. (d) Effective $M(D^{*\pm}K^0_S)$ distribution (full dots). The solid line is a fit to a Gaussian resonance plus background of the form $A(\Delta M^{ext})^B$.

$203 \pm 60$, respectively.

The acceptance-corrected fractions of $D^{*\pm}$ mesons originating from $D^0_1$ and $D^{*0}_2$ in the measured kinematic range were found to be $R_{D^0_1 \to D^{*\pm}\pi^\mp / D^{*\pm}} = 3.40 \pm 0.42\,(\text{stat.})^{+0.78}_{-0.63}\,(\text{syst.})\%$ and $R_{D^{*0}_2 \to D^{*\pm}\pi^\mp / D^{*\pm}} = 1.37 \pm 0.40\,(\text{stat.})^{+0.96}_{-0.33}\,(\text{syst.})\%$. Extrapolating to the full kinematic phase space by a MC simulation and using the partial width ratio, $\Gamma(D^{*0}_2 \to D^+\pi^-)/\Gamma(D^{*0}_2 \to D^{*+}\pi^-) = 2.3 \pm 0.6$ [23], the rate of c quarks hadronising as $D^{*+}$ mesons, $f(c \to D^{*+}) = 0.235 \pm 0.007 \pm 0.007$ [9], and isospin conservation, the rates of c quarks hadronising as $D^0_1$ and $D^{*0}_2$ mesons are found to be: $f(c \to D^0_1) = 1.46 \pm 0.18\,(\text{stat.})^{+0.33}_{-0.27}\,(\text{syst.}) \pm 0.06\,(\text{ext.})\%$ and $f(c \to D^{*0}_2) = 2.00 \pm 0.58\,(\text{stat.})^{+1.40}_{-0.48}\,(\text{syst.}) \pm 0.41\,(\text{ext.})\%$. The third errors arise from uncertainties in $f(c \to D^{*+})$ and the $D^{*0}_2 \to D^{*+}\pi^-$ branching ratio. The results are consistent with the $e^+e^-$ rates measured by CLEO [26]: $f(c \to D^0_1) = 1.8 \pm 0.3\%$ and $f(c \to D^{*0}_2) = 1.9 \pm 0.3\%$.

## Search for radially excited $D^{*\prime\pm}$

Radially excited charm mesons with mass around $2.6\,\text{GeV}$ are predicted [27] to decay into $D\pi\pi$ or $D^*\pi\pi$. A narrow resonance in the $D^{*\pm}\pi^+\pi^-$ final state at $2637\,\text{MeV}$, interpreted as the radially excited $D^{*\prime\pm}$, was reported by DELPHI [28]. No evidence

for this state has been found by OPAL and CLEO [29].

$D^{*\prime\pm}$ candidates were reconstructed by ZEUS [25] from their decays to $D^{*\pm}\pi_4^+\pi_5^-$. No narrow resonance is seen in the extended mass difference $M(K\pi\pi_S\pi_4\pi_5) - M(K\pi\pi_S) + M(D^*)$. An upper limit of $R_{D^{*\prime+}\to D^{*+}\pi^+\pi^-/D^{*+}} < 2.3\%$ $(95\%\ C.L.)$ is obtained in the measured kinematic region for the fraction of $D^{*\pm}$ originating from $D^{*\prime\pm}$ decays within a signal window $2.59 < M(D^{*\prime\pm}) < 2.67\,\text{GeV}$, which covers theoretical predictions [27] and the DELPHI measurement [28]. Extrapolating by a MC simulation to the full kinematic phase space and using the known $f(c \to D^*)$ value, a $D^{*\prime\pm}$ production limit of $f(c \to D^{*\prime+}) \cdot B_{D^{*\prime+}\to D^{*+}\pi^+\pi^-} < 0.7\%$ $(95\%\ C.L.)$ is obtained. A similar limit of $0.9\%$ has been reported by OPAL [30].

## Production of the charm-strange meson $D_{s1}^{\pm}(2536)$

$D_{s1}^{\pm}$ mesons were reconstructed by ZEUS [5] via the $D^{*\pm}K_S^0$ decay mode with $K_S^0 \to \pi^+\pi^-$. $K_S^0$ candidates were identified by using pairs of oppositely charged tracks with $p_\perp > 0.2\,\text{GeV}$. A clean $K_S^0 \to \pi_3\pi_4$ signal was extracted after applying standard $V^0$-finding cuts. $K_S^0$ candidates with $0.480 < M(\pi_3\pi_4) < 0.515\,\text{GeV}$ were kept for the $D_{s1}^{\pm}$ reconstruction. Fig. 5(d) shows the effective $M(D^{*\pm}K_S^0)$ distribution in terms of $\Delta M^{ext} + M(D^{*+})_{PDG} + M(K^0)_{PDG}$ (solid dots), where $\Delta M^{ext} = M(K\pi\pi_S\pi_3\pi_4) - M(K\pi\pi_S) - M(\pi_3\pi_4)$ and $M(D^{*+})_{PDG}$ ($M(K^0)_{PDG}$) is the nominal $D^{*\pm}$ ($K^0$) mass [23]. A clear signal is seen at the $M(D_{s1}^{\pm})$ value. The solid curve is an unbinned likelihood fit to a Gaussian resonance plus background of the form $A(\Delta M^{ext})^B$. The fit yielded $62.3 \pm 9.3$ $D_{s1}^{\pm}$ mesons. The mass value was found to be $M(D_{s1}^{\pm}) = 2534.2 \pm 0.6 \pm 0.5\,\text{MeV}$, in rough agreement with the PDG value [23]. The last error is due to the uncertainty in $M(D^{*+})_{PDG}$.

The angular distribution of the $D_{s1}$ signal was studied via the helicity angle, $\alpha$, between the $K_S^0$ and $\pi_S$ momenta in the $D^{*\pm}$ rest frame. The $dN/d\cos\alpha$ distribution was fitted to $(1 + R\cos^2\alpha)$. An unbinned likelihood fit yielded $R = -0.53 \pm 0.32\,(\text{stat.})^{+0.05}_{-0.14}\,(\text{syst.})$, consistent with the CLEO value [31] $R = -0.23^{+0.40}_{-0.32}$. Both measurements are consistent with $R = 0$, i.e. $J^P = 1^+$ for the $D_{s1}$ meson. However, our result is not inconsistent with $R = -1$, i.e. $J^P = 1^-$ or $2^+$ [32].

The fraction of $D^{*\pm}$ mesons originating from $D_{s1}^{\pm}$ in the measured kinematic region is $R_{D_{s1}^{\pm}\to D^{*\pm}K^0/D^{*\pm}} = 1.77 \pm 0.26\,(\text{stat.})^{+0.11}_{-0.09}\,(\text{syst.})\%$. The rate of c quarks hadronising as $D_{s1}^+$ mesons, after a MC extrapolation to the full kinematic phase space, is $f(c \to D_{s1}^+) = 1.24 \pm 0.18\,(\text{stat.})^{+0.08}_{-0.06}\,(\text{syst.}) \pm 0.14\,(\text{br.})\%$. The third error is due to uncertainties in $f(c \to D^{*+})$ and the $D_{s1}^+ \to D^{*+}K^0$ branching ratio. The rate agrees with the OPAL value [33] $1.6 \pm 0.4 \pm 0.3\%$. This rate is about twice that expected, assuming $f(c \to D_1^0) \approx 2\%$ [25] and $\gamma_s \approx 0.3$ [8], where $\gamma_s$ is the strangeness suppression factor in charm production.

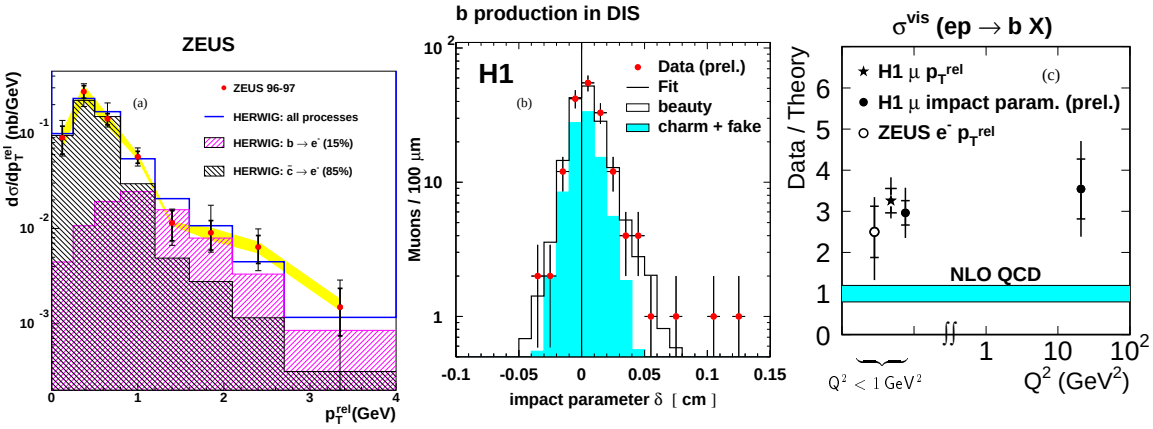


**FIGURE 6.** (a) Differential cross section in $p_T^{rel}$ for the production of electrons in dijet PHP events compared to HERWIG MC shape prediction (solid line). The MC beauty (charm) component is given by the forward- (backward-) diagonally hatched histogram. (b) Muon impact parameter, $\delta$, distribution for DIS events, with a likelihood fit decomposition into beauty (white region) and charm + fake (shaded region). (c) Ratio of measured $b$ production cross sections over theoretical expectation, as a function of $Q^2$. The shaded band represents the theoretical uncertainty.

## OPEN BEAUTY PRODUCTION

The production rates for beauty at HERA are about two orders of magnitude smaller than for charm. Theoretical uncertainties are expected to be smaller due to the high $b$ quark mass. Enriched $b$ samples have been obtained [34, 35, 36, 37] by studying electrons or muons from semileptonic (SL) $b$ decays. Due to the heavy $b$ quark, the high tail of the lepton $p_T$ with respect to the axis of the closest jet, $p_T^{rel}$, provides a $b$ signature. H1 has also exploited, using their micro-vertex detector, the long lifetimes of $b$ hadrons to extract $b$ production cross sections by measuring the impact parameter, $\delta$, which is the distance of closest approach of SL muons to the primary vertex in the plane transverse to the beam axis.

The ZEUS differential cross section, $d\sigma/dp_T^{rel}$, for a PHP dijet event sample of $\mathcal{L} = 38.5\,\text{pb}^{-1}$ with identified electrons is compared in Fig. 6(a) [35] with a MC $c$ and $b$ production simulation. The shape is fitted by varying the relative contributions of $c$ and $b$. A $b$ fraction of $\approx 15\%$ is obtained, consistent with the MC expectation.

For a PHP dijet sample with an identified muon, H1 has shown [36] that the $p_T^{rel}$ and $\delta$ methods provide independent and consistent $b$ production results. The H1 analysis of a smaller DIS sample from $\mathcal{L} = 10.5\,\text{pb}^{-1}$ [37] uses the combination of the two observables. A likelihood fit of $b\bar{b}$, $c\bar{c}$ and fake muon spectra to a two-dimensional distribution in $\delta$ and $p_T^{rel}$ adjusts the relative weights of all three components in the data. It yields a $b\bar{b}$ fraction of $(43 \pm 8)\%$. The $\delta$ projection of this distribution is shown in Fig. 6(b) together with the fit decomposition.

The ratio of the measured visible $b$ cross sections over theoretical expectations [10, 17] is shown in Fig. 6(c) as a function of $Q^2$ [37]. The ratio is roughly constant with $Q^2$ and the discrepancy between data and NLO calculations is quite significant. The DIS case is theoretically cleaner, since at high $Q^2$ the resolved contribution is expected to be suppressed.

# REFERENCES


1. S. Frixione et al., Nucl. Phys. B412 (1994) 225;
   M. Mangano et al., Nucl. Phys. B373 (1992) 295.
2. R.K. Ellis and P. Nason, Nucl. Phys. B 312 (1989) 551;
   P. Nason, S. Dawson and R.K. Ellis, Nucl. Phys. B 303 (1988) 607;
   J. Smith and W.L. van Neerven, Nucl. Phys. B 374 (1992) 36.
3. B.A. Kniehl et al., Z. Phys. C76 (1997) 689;
   J.Binnewies et al., Z. Phys. C76 (1997) 677; Phys. Rev. D58 (1998) 014014.
4. M. Cacciari et al., Z. Phys. C69 (1996) 459; Phys. Rev. D55 (1997) 2736;
   M. Cacciari and M. Greco, Phys. Rev. D55 (1997) 7134.
5. ZEUS Collaboration, paper 497 submitted to EPS Conf. on HEP2001, Budapest, Hungary.
6. ZEUS Collaboration, paper 501 submitted to EPS Conf. on HEP2001, Budapest, Hungary.
7. OPAL Collaboration, K. Ackerstaff et al., Eur. Phys. J. C 5 (1998) 1;
   ALEPH Collaboration, R. Barate et al., Eur. Phys. J. C 16 (2000) 597.
8. ZEUS Collaboration, J. Breitweg et al., Phys. Lett. B481 (2000) 213.
9. L. Gladilin, hep-ex/9912064.
10. B.W. Harris and J. Smith, Phys. Rev. D57 (1998) 2806;
    E. Laenen et al., Nucl. Phys. B392 (1995) 162.
11. ZEUS Collaboration, paper 449 submitted to XXX ICHEP2000, Osaka, Japan.
12. ZEUS Collaboration, paper 493 submitted to EPS Conf. on HEP2001, Budapest, Hungary.
13. H1 Collaboration, C. Adloff et al., hep-ex/0108039, submitted to Phys. Lett. B (2001).
14. H. Jung and G.P. Salam, Eur. Phys. J. C19 (2001) 351; H. Jung, hep-ph-0109146.
15. M. Ciafaloni, Nucl. Phys. B296 (1988) 49;
    S. Catani et al., Phys. Lett. B234 (1990) 339; Nucl. Phys. B 336 (1990) 18;
    G. Marchesini, Nucl. Phys. B445 (1995) 49.
16. ZEUS Collaboration, Breitweg J. et al., Eur. Phys. J. C6 (1999) 67.
17. S. Frixione et al., Nucl. Phys. B454 (1995) 3 ; Phys. Lett. B348 (1995) 633.
18. A.V. Berezhnoy, V.V. Kiselev, and A.K. Likhoded, hep-ph/9901333, hep-ph/9905555, Yad. Fiz. [Phys. At. Nucl.] in print (2000).
19. ZEUS Collaboration, paper 495 submitted to EPS Conf. on HEP2001, Budapest, Hungary.
20. G. Ingelman et al., Comp. Phys. Comm. 101 (1997) 135.
21. V. Gribov and L. Lipatov, Sov. J. Nucl. Phys. 15 (1972) 438; ibid. 15 (1972) 675;
    L. Lipatov, Sov. J. Nucl. Phys. 20 (1975) 94;
    G. Altarelli and G. Parisi, Nucl. Phys. B126 (1977) 298;
    Y. Dokshitser, Sov. Phys. JETP 46 (1977) 641.
22. ZEUS Collaboration, paper 499 submitted to EPS Conf. on HEP2001, Budapest, Hungary.
23. Particle Data Group, D. E. Groom et al., Eur. Phys J C15 (2000) 1.
24. N. Isgur and M.B. Wise, Phys. Lett. B232 (1989) 113;
    M. Neubert, Phys. Rep. A245 (1994) 259.
25. ZEUS Collaboration, paper 448 submitted to XXX ICHEP2000, Osaka, Japan.
26. CLEO Collaboration, Avery P. et al., Phys. Lett. B331 (1994) 236.
27. S. Godfrey and N. Isgur, Phys. Rev. D32 (1985) 189;
    D. Ebert et al., Phys. Rev. D57 (1998) 5663.
28. DELPHI Collaboration, P. Abreu et al., Phys. Lett. B426 (1998) 231.
29. OPAL Collaboration, XXIX ICHEP1998, Vancouver, Canada;
    CLEO Collaboration, hep-ex/9901008.
30. OPAL Collaboration, hep-ex/0101045, submitted to Eur. Phys. J. C (April 2001).
31. CLEO Collaboration, J.P. Alexander et al., Phys. Lett. B303 (1993) 303.
32. S. Godfrey and R. Kokoski, Phys. Rev. D43 (1991) 1130.
33. OPAL Collaboration, K. Ackerstaff et al., Z. Phys. C76 (1997) 425.
34. H1 Collaboration, C. Adloff et al., Phys. Lett. B467 (1999) 156.
35. ZEUS Collaboration, J. Breitweg et al., Euro. Phys. J. C18 (2001) 625.
36. H1 Collaboration, abstract 982 submitted to XXX ICHEP2000, Osaka, Japan.
37. H1 Collaboration, paper 807 submitted to EPS Conf. on HEP2001, Budapest, Hungary.